Seasonal-Latitudinal Structure of the Diurnal Thermospheric Tide

JEFFREY M. FORBES

Space Data Analysis Laboratory, Boston College, Chestnut Hill, Mass., 02159, and Center for Earth and Planetary Physics, Harvard University, Cambridge, Mass. 02138

HENRY B. GARRETT

Space Physics Division, Air Force Geophysics Laboratory, Hanscom AFB, Bedford, Mass. 01730

(Manuscript received 16 June 1977, in final form 5 October 1977)

ABSTRACT

The seasonal-latitudinal structure of the diurnal thermospheric tide is investigated for minimum and maximum levels of solar activity by numerically solving the linearized inseparable tidal equations for a spherical, rotating, viscous atmosphere with anisotropic ion drag. Variations in F-region ionospheric structure and the solar zenith angle dependence of the EUV heat source are major factors controlling the seasonal-latitudinal structure of the diurnal thermospheric tide. The combined interaction of the solar-cycle dependent background temperature profile (which controls the altitude of diffusion dominance) and variations in the seasonal structure of the ionospheric plasma with sunspot activity leads to a solar-cycle variation of the seasonal-latitudinal morphology of the diurnal tide. For instance, summer-winter differences in tidal winds at a given height are more prouounced during SSMAX as opposed to SSMIN. At a given level of solar activity, westerly winds, vertical winds and temperatures are generally larger in the summer hemisphere, whereas the amplitude of the northerly wind is greatest during winter. There also exist summer-winter phase differences in the tidal fields ranging from 1 to 6 h, depending upon height, latitude and sunspot activity. Computations of diurnal oscillations in O and N_2 are presented which similarly demonstrate a complex dependence of tidal effects on height, latitude, season and solar activity. In particular, the temperature-atomic oxygen phase difference (the so-called "phase anomaly") at 300 km varies from about 7 to -2 h at SSMAX and 2 to -2 h at SSMIN, between 80°S and 80°N, respectively, at December solstice. The above results suggest that related seasonal-latitudinal and solar-cycle variations exist in midlatitude ionospheric structure, the F-region equatorial anomaly, the tidal distributions of O_2, Ar, He and H, and magnetic and electric fields generated by the E-region dynamo mechanism. Finally, it is concluded that static diffusion models based on families of empirical temperature profiles cannot simultaneously yield realistic diurnal variations in O, N_2 *and* temperature below 200 km for SSMIN and 300 km for SSMAX.

1. Introduction

The accumulation of extensive composition and total mass density data from *in situ* satellite experiments (Hedin *et al.*, 1974; Marcos *et al.*, 1977), the increasing abundance of incoherent scatter measurements of temperature and winds (Amayenc, 1974; Salah, 1974; Roble *et al.*, 1974), and the development of sophisticated numerical models (Volland and Mayr, 1973; Harris and Mayr, 1975; Dickinson *et al.*, 1975; Straus *et al.*, 1975a,b; Hong and Lindzen, 1976; Forbes and Garrett, 1976), have all contributed to an upsurge in our understanding of the quiet-time meteorology of the thermosphere (roughly above 100 km). Previous theoretical work on semidiurnal tides, diurnal tides and the zonally averaged thermospheric circulation are summarized by Hong and Lindzen (1976), Forbes and Garrett (1976) and Dickinson *et al.* (1975), respectively. Recently, the present authors (Garrett and Forbes, 1978) have calibrated the upward propagating semidiurnal tidal structures with incoherent scatter measurements, superimposed the thermospheric extensions of these fields upon the diurnal and semidiurnal components excited *in situ*, and investigated the local time structure of the thermospheric temperature and winds as a function of altitude, latitude and solar cycle under equinox conditions.

The seasonal-latitudinal structure of the *total* thermospheric tidal response, consisting of higher order harmonics in addition to the diurnal tide, is likely to be significantly affected by the (2,3) and (2,5) asymmetric semidiurnal modes excited in the mesosphere and below (Hong and Lindzen, 1976; Lindzen, 1976), particularly during low solar activity when the *in situ* contribution is less. The *structures* of the extensions of these modes into the thermo-

0022-4928/78/0148-0159$06.00

sphere, in addition to the (2,2) and (2,4) modes, have been computed by the present authors in unpublished work in the manner outlined by Hong and Lindzen (1976). However, uncertainties in the zonally averaged mesospheric wind distribution (responsible for mode coupling) and in the direct excitation sources make absolute specification of the antisymmetric semidiurnal fields difficult. Furthermore, insufficient solstice data are available to reliably perform the multiple-station calibration necessary to determine the amplitudes and phases of the symmetric and antisymmetric components. On the other hand, the diurnal thermospheric tide is excited almost exclusively *in situ* (Forbes and Garrett, 1976), and observational data are plentiful for a reasonably accurate calibration of the EUV heat source. Since the EUV flux does not vary with season, investigation of solstice conditions only requires a transformation of the earth-sun geometry and appropriate modeling of seasonal variations in the background (zonally averaged) atmospheric and ionospheric structures. It appears, then, that a study of the seasonal component of the diurnal thermospheric tide would be fruitful at the present time, whereas investigation of semidiurnal or higher order effects must await further observational data to perform a proper calibration.

The present paper concentrates on the structure of the seasonal component of the diurnal thermospheric tide, and the variation of the seasonal-latitudinal morphology with solar cycle. In particular, the effects of the tidal dynamics on the distributions of O and N_2 below 500 km are computed, revealing the seasonal-latitudinal and solar-cycle dependence of the so-called "phase anomaly" between upper atmosphere temperature and density, and other effects of wind-induced diffusion on the density structure of the thermosphere. The tidal winds presented here also provide useful inputs to models of ionospheric structure (Roble, 1975) and the E-region dynamo (Forbes and Lindzen, 1976; Richmond *et al.*, 1976), and should provide some insight into the seasonal and solar-cycle morphology of the midlatitude ionosphere, of the equatorial F-region anomaly, and of the ground magnetic variations due to the Sq current system. In addition, forthcoming lower thermosphere data from *in situ* experiments aboard Atmosphere Explorer C, D and E will require theoretical models of tidal dynamics to aid in interpretive analyses and the construction of models of ionospheric chemistry where transport by neutral winds is important. In contrast to the present method, wind estimates in the lower thermosphere (below 250 km) by using pressure gradients from empirical static diffusion models as forcing terms in the horizontal momentum equations of the neutral gas (Kohl and King, 1967; Geisler, 1967; Roble and Dickinson, 1974) are inadequate, since the empirical models do not delineate many important structural features below 250 km due to scarcity of data with adequate spatial and temporal resolution.

2. The model

a. Tidal dynamics

Since the present work is essentially a continuation of the Forbes and Garrett (1976) study (hereafter referred to as Paper I), the reader is referred there for mathematical details and numerical method of solution. Briefly, the diurnal thermospheric tide excited by *in situ* absorption of EUV and UV solar radiation is determined by numerically integrating the linearized tidal equations for a spherical, rotating, viscous atmosphere. The model takes into account eddy viscosity, Newtonian cooling, molecular viscosity and conductivity, Coriolis acceleration and anisotropic ion drag. A departure from the numerical scheme in Paper I is that the integration is now performed pole to pole, rather than adopting symmetry conditions at the equator. Furthermore, some modifications have been made in the thermal excitation and ion drag models, which are outlined in the following.

The values quoted by Hilsenrath *et al.* (1960) and Roble and Dickinson (1973) indicate that a more realistic choice of the thermal conductivity, represented by $K=K_0T^{\frac{1}{2}}/M$, where T is the temperature K and M the mean molecular weight g mol^{-1}, is given by $K_0=0.042$ J K^{-1} m^{-1} s^{-1}, rather than the value $K_0=0.0158$ J K^{-1} m^{-1} s^{-1} adopted in Paper I. From unpublished calculations of the globally averaged thermospheric structure, we note here that the choice of thermal conductivity is not nearly so sensitive with respect to tidal calculations as in the computation of the mean thermospheric structure. The above modification requires 25% increases in the solar heat inputs of Paper I to $\overline{\epsilon F}_\infty \approx 0.50$ erg cm^{-2} s^{-1} at SSMIN and $\overline{\epsilon F}_\infty \approx 1.0$ erg cm^{-2} s^{-1} at SSMAX to maintain consistency with the observed diurnal thermospheric oscillation as determined from satellite drag measurements (Jacchia and Slowey, 1968).

The seasonal-latitudinal structure of the EUV and UV heat sources are modeled by the Chapman function zenith angle dependence (Rishbeth and Garriott, 1969) represented by

$$q_{\text{diurnal}} = f q_{\max} \exp[1 - z - \text{Ch}(\chi,z)\, e^{-z}],$$

where $\text{Ch}(\chi,z)$ is the Chapman function, $z=(x-x_{\max})/\delta x$ the distance in scale heights above the peak for an overhead sun ($\chi=0$), $q_{\max}$ the peak heating rate for $\chi=0$ and f the fraction of total heating going into diurnal excitation. Values of $x_{\max}=19.47$ and $x_{\max}=16.1$ are adopted for the EUV and UV heat sources, respectively. The EUV and UV peak heating rates are, respectively, 1.0×10^{-8} and 4.0×10^{-7} J m^{-3} s^{-1} at SSMIN, and 1.25×10^{-8} and 6.0×10^{-7} J

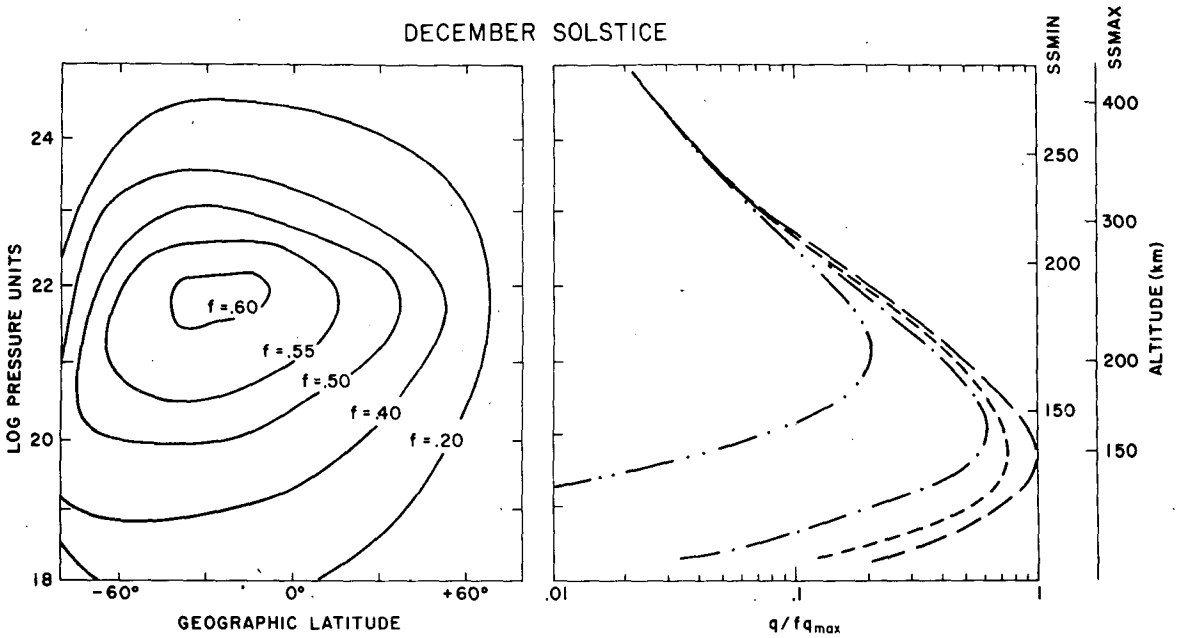

FIG. 1. Left: fraction f of total heating going into diurnal excitation, as determined by Fourier analysis with respect to local time. Right: the function $\exp[1-z-\mathrm{Ch}(\chi,z)e^{-z}]$, defined in the text, at latitudes $-30°$ (——), $-60°$ (– – –), $+30°$ (—·—), and $+60°$ (—··—). December solstice conditions are assumed.

m^{-3} s^{-1} at SSMAX. Profiles of f and $q_{\text{diurnal}}/fq_{\max}$ for the EUV contribution are plotted in Fig. 1, demonstrating seasonal-latitudinal variations in the local-time structure of the diurnal EUV heating, as well as in the vertical structure.

Calculation of the thermal excitation does not assume the zonally averaged distribution of the absorbing gases to vary with latitude, however, as a consistent tidal calculation would require inclusion of mean wind and temperature distributions which are height and latitude dependent. Instead, it is assumed that the background neutral atmosphere is motionless and a function of altitude only. Inclusion of these effects in the present model must await more comprehensive descriptions of the zonally averaged wind, temperature and composition distributions than is currently available.

In Paper I a simple analytic model of the ion drag force is described, where the relevant parameters are the critical frequency of the F-layer (f_0F_2), the height of f_0F_2 (h_mF_2) and the F-layer slab thickness (Y_mF_2, assumed equal to twice the neutral scale height). Values of f_0F_2 and h_mF_2 were chosen to describe the salient features of the latitude and solar cycle variations of the F-region ionosphere. However, since the ionospheric model of Ching and Chiu (1973) is widely used in other dynamical calculations of the thermosphere (cf. Dickinson *et al.*, 1975; Straus *et al.*, 1975a,b), we have in the interest of consistency also adopted the Ching and Chiu model [and subsequent modifications (Ching, 1975)] in our numerical simulations. A comparison of equinox calculations using the Ching and Chiu model with those presented in Paper I showed little difference in the results, indicating that *detailed* specification of ionospheric structure is unnecessary in this type of large-scale dynamical calculation. The relevant gross features of the seasonal-latitudinal variability in ionospheric structure for our purposes are as follows:

1) At midlatitudes, winter noon f_0F_2 is 50–100% greater than summer noon f_0F_2 (the F-region winter anomaly).

2) For both SSMIN and SSMAX at midnight, summer f_0F_2 is 50–100% greater than winter f_0F_2.

3) The winter anomaly is virtually absent during SSMIN.

As discussed in Paper I, the important parameter relating momentum coupling between the ionized and neutral gases relevant to diurnal tidal oscillations is the longitude- and local-time averaged ion drag coefficient $\bar{\nu}_0$, defined in Paper I. Values of $\bar{\nu}_0$ at each point in the latitude-height grid were computed from the Ching and Chiu (1973) model. Representative profiles are depicted in Fig. 2 which reflect the influence of (1)–(3) above on the quantity $\bar{\nu}_0$. Ramifications of seasonal variations in ionospheric structure on the tidal fields are discussed in Section 3.

b. Composition variations

The thermosphere consists predominantly of atomic oxygen between 200 and 500 km, and this species therefore plays a major role in explaining total mass

density variations derived from satellite drag data. It is well known (i.e., Mayr and Volland, 1972, 1973) that winds play an important part in determining the distribution of atomic oxygen in the thermosphere. As discussed in Forbes and Garrett (1976), tidal solutions asymptote to their diffusion-dominated values below the level where $[O]\sim[N_2]$ implying that the temperature and wind fields can be computed without taking into account variations in the relative composition at any given height, and the composition variations computed *a posteriori* through diffusive forcing. This procedure has been justified by Mayr and Volland (1973) using a simplified binary gas (O-N_2) model, where it is demonstrated that the approximation leads to order 10% errors in the diurnal temperature amplitude.

By combining the linearized vertical momentum equation

$$w_i = w - D\frac{\partial}{\partial h}\Delta \ln N_i - \alpha D \tag{1}$$

and continuity equation

$$\Delta \ln N_i = \frac{i}{n\Omega}\left\{\nabla\cdot\mathbf{V} + \beta w_i + \frac{\partial w_i}{\partial h} + K[Y]'\right\} \tag{2}$$

for a single thermospheric constituent, it may be shown that the tidal variations of the ith constituent are governed by

$$\frac{\partial^2 R_i}{\partial h^2} + \left(\beta + \frac{1}{D}\frac{\partial D}{\partial h}\right)\frac{\partial R_i}{\partial h} + \frac{n\Omega}{iD}R_i = \frac{1}{D}\left\{\nabla\cdot\mathbf{V} + \beta w - \alpha\beta D - \frac{\partial}{\partial h}\alpha D + \frac{\partial w}{\partial h} + K[Y]'\right\}, \tag{3}$$

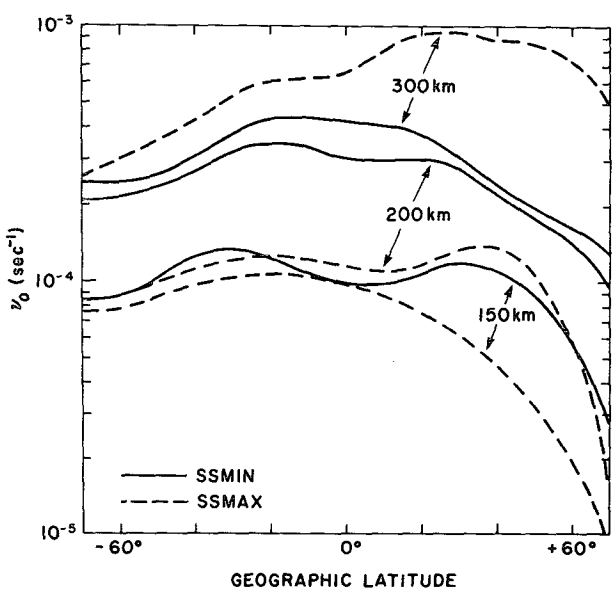

FIG. 2. Diurnally and longitudinally averaged ion drag coefficient $\bar{\nu}_0$ as a function of geographic latitude at several heights and levels of solar activity for December solstice conditions.

where

R_i	tidal variation in $N_i[=\Delta \ln N_i]$
$\ln N_i$	$\ln N_{i0}+\Delta \ln N_i$
N_i	number density of ith constituent
N_{i0}	background (globally averaged) distribution of ith constituent
β	$-\frac{(1+\alpha_i)}{T_0}\frac{\partial T_0}{\partial h}-\frac{1}{H_{i0}}-\frac{\phi_{i0}}{DN_{i0}}$
α_i	thermal diffusion coefficient (equal to zero for O, N_2, Ar and O_2)
T_0	background temperature
H_{i0}	background scale height for ith constituent
ϕ_{i0}	vertical flux of ith constituent in background atmosphere due to chemical production and loss or Jeans escape
D	diffusion coefficient
Ω	rotation rate of earth
n	zonal wavenumber
$\nabla\cdot\mathbf{V}$	divergence of horizontal tidal velocity field
w	perturbation vertical velocity of background gas
w_i	perturbation vertical velocity of ith constituent
α	$(1+\alpha_i)\left[\frac{1}{T_0}\frac{\partial T'}{\partial h}-\frac{T'}{T_0^2}\frac{\partial T_0}{\partial h}\right]-\frac{H_i'}{H_{i0}^2}$
T'	tidal perturbation of temperature
H_i'	tidal perturbation of scale height for ith constituent
$K[Y]'$	production or loss rate through chemical reaction between N_i and some constituent Y
h	altitude.

In addition it is assumed that the background distribution is given by

$$\frac{dN_{i0}}{dh} + \frac{N_{i0}}{H_{i0}} + N_{i0}\frac{(1+\alpha_i)}{T_0}\frac{dT_0}{dh} = -\frac{\phi_{i0}}{D} \tag{4}$$

with solution

$$N_{i0}(h) = \left[N_{i0}(h_0) - \int_{h_0}^{h}\frac{\phi_{i0}}{D}\left(\frac{T_0(h)}{T_0(h_0)}\right)^{1+\alpha_i} e^{Z_i} dh\right] \times \left(\frac{T_0(h_0)}{T_0(h)}\right)^{1+\alpha_i} e^{-Z_i}, \tag{5}$$

where

$$Z_i = -\int_{h_0}^{h}\frac{dh'}{H_{i0}}.$$

The work of Mayr and Harris (1977) shows that tidal variations of O are only weakly dependent on

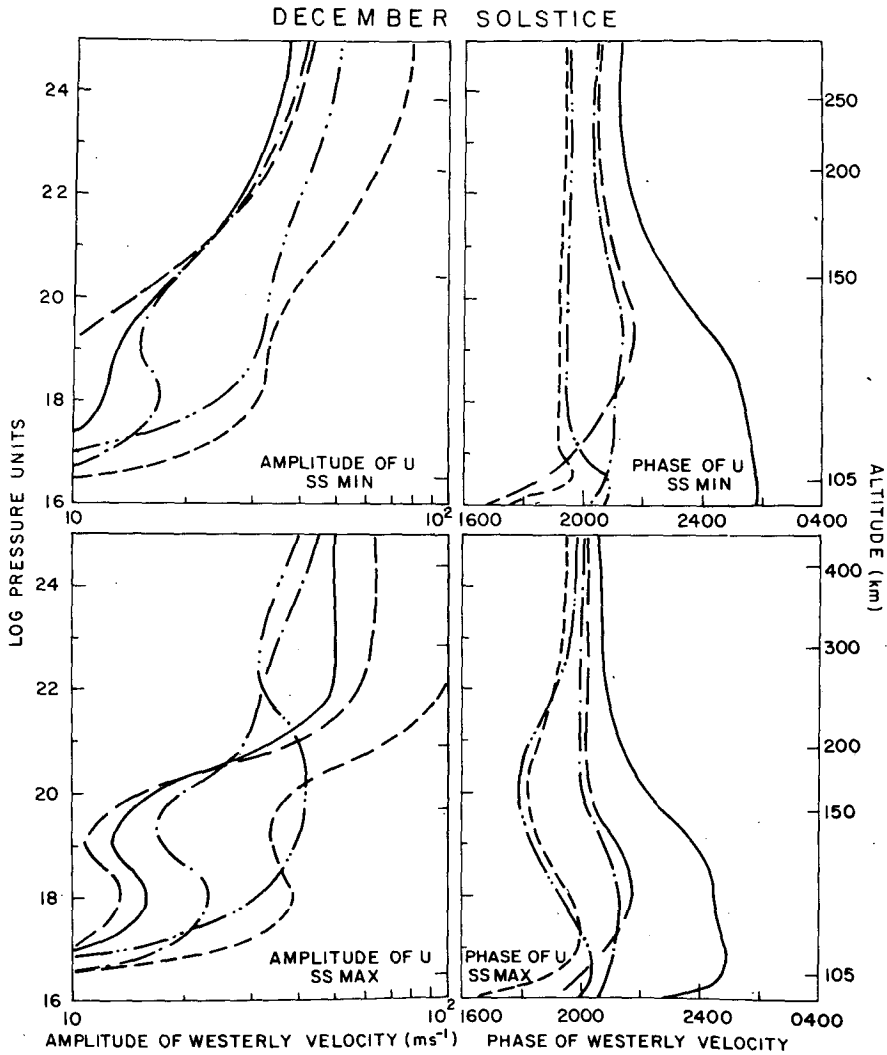

FIG. 3. Vertical profiles of westerly velocity for SSMIN (top) and SSMAX (bottom) at latitudes −60° (– – –), −30° (— — —), 0° (——), +30° (—·—), and +60° (—··—), for December solstice conditions.

photoproduction and chemical loss mechanisms above 150 km. Therefore, Φ_{i0} and K may be set equal to zero in the above formulations when considering tidal variations of O and N_2 above 150 km. In this paper we restrict our attention to O and N_2 variations; consideration of diurnal and semidiurnal variations in O, O_2, N_2, Ar, He, and H will be treated in a forthcoming article.

For O and N_2, boundary conditions for (1) are $R_i=0$ at the lower boundary ($h\approx100$ km) and diffusive equilibrium at the upper boundary ($h\approx300$ km at SSMIN and $h\approx440$ km at SSMAX): $\partial R_i/\partial h=-\alpha$. Eq. (1) is solved numerically using the Lindzen and Kuo (1969) algorithm for Gaussian elimination.

3. Results and comparison with observations

a. Tidal fields

The solar cycle variability of diurnal wind and temperature structures at equinox are analyzed in Forbes and Garrett (1976). Since the important results to emerge from that study also apply to winter and summer conditions, the reader is referred there for more extensive interpretation. The major results are summarized as follows:

1) Amplitudes and phases of horizontal velocity and temperature asymptote to constant values in the upper thermosphere. This occurs at a lower altitude during SSMIN than SSMAX, since the level of diffusion dominance occurs at a lower level when the mean exospheric temperature is less.

2) Vertical structures of amplitude and phase vary with latitude. This feature results from the inseparability of the system imposed by the joint presence of diffusion and rotation, and the latitude-height dependence of the ion drag coefficient.

3) While the solar heat input increases by a factor of 2 from SSMIN to SSMAX, temperature amplitudes

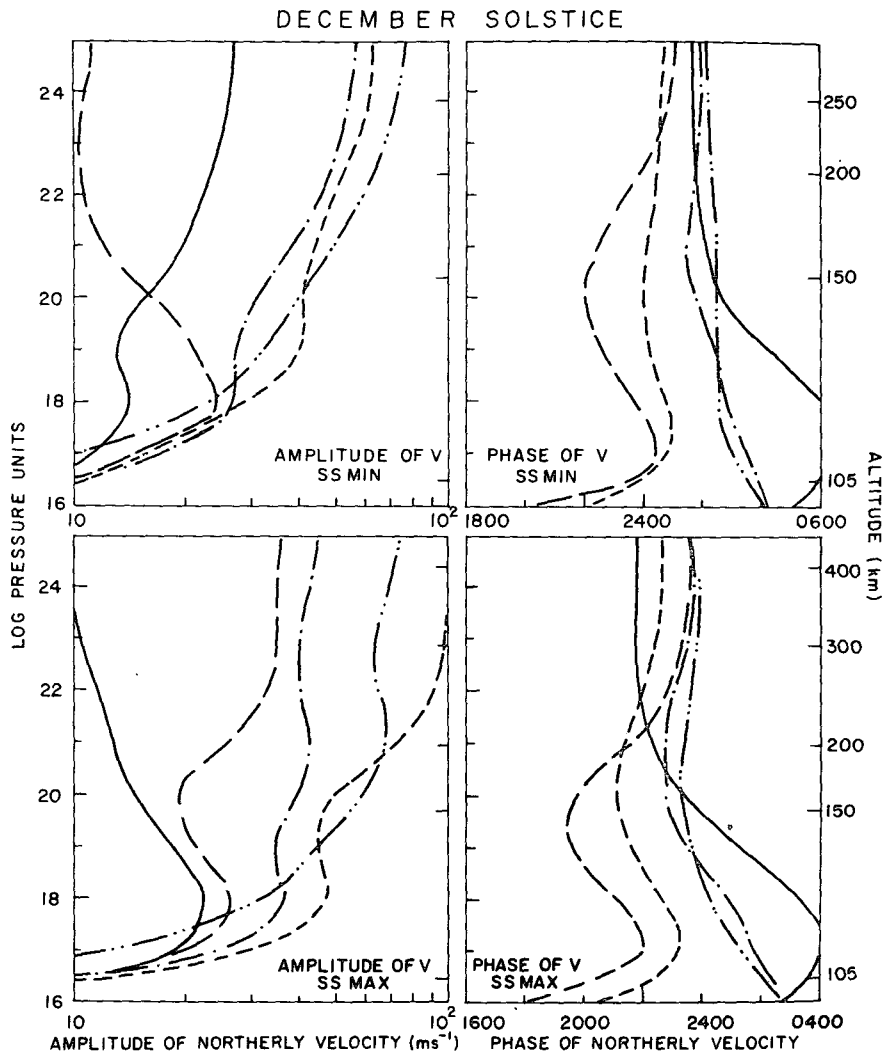

FIG. 4. As in Fig. 3, except for northerly velocity. Southern Hemisphere phases are shifted by 12 h for convenience of illustration.

are roughly a factor of 3 greater during SSMAX, whereas the velocity amplitudes are comparable at SSMIN and SSMAX. This results in part from the increased deceleration of winds due to ion drag during SSMAX, which in turn affects the adiabatic heating and cooling to give the above result.

In the following, summer-winter *asymmetries* in the diurnal tidal structures are analyzed for minimum and maximum levels of solar activity. As in Paper I, sunspot minimum conditions (SSMIN) are represented by a global mean exospheric temperature of 800 K (sunspot number $R \approx 10$), and sunspot maximum conditions (SSMAX) by 1400 K ($R \approx 180$).

Vertical profiles of westerly and northerly winds at 30° increments of latitude are plotted in Figs. 3 and 4, respectively, at December solstice. One feature which can be inferred from these figures is that summer-winter differences in the horizontal velocity field at a given height and latitude are generally greater during SSMAX than SSMIN. There are factors relating to the physics of the problem which can be identified to support this observation. First, the diurnally and longitudinally averaged ion drag coefficient $\bar{\nu}_0$ is larger and more variable with respect to season during SSMAX as opposed to SSMIN (cf. Fig. 2). Furthermore, since the tidal fields asymptote to their diffusion-dominated values at a lower altitude during SSMIN, they would therefore be less affected by variations in F-region structure. Summer-winter phase differences at a given height are about the same during SSMIN and SSMAX, being on the order of 1–4 h for northerly velocity and usually less than $\frac{1}{2}$ h for westerly velocity.

By performing numerical simulations using a symmetric (equinox) $\bar{\nu}_0$ distribution, some further insight into the cause-effect relationship between the ion

drag effect and seasonal-latitudinal variations in tidal structures was obtained. Basically, for a given level of solar activity, the ion drag influence on the seasonal variability of the northerly and westerly velocity fields is straightforward; higher values of $\bar{\nu}_0$ act to further decelerate the horizontal velocity fields, resulting from transfer of momentum from the neutral gas by collisional interaction with the ionized constituents. However, the fact that $\bar{\nu}_0$ above 200 km is greatest in the summer hemisphere during SSMIN, and winter hemisphere during SSMAX leads to a solar cycle variation of the seasonal-latitudinal morphology. During SSMIN, seasonal variations in F-region structure reinforce seasonal variations in westerly velocity due to the zenith angle dependence of the EUV heat source at all latitudes, and tend to diminish the seasonal variation in northerly velocity at low to midlatitudes. On the other hand, the ion drag effect during SSMAX results in slightly less variability in westerly velocity at all latitudes and northerly velocity at high latitudes, and a greater variation in northerly velocity at low to midlatitudes.

Incoherent scatter measurements near 45°N (Amayenc, 1974; Roble *et al.*, 1977) indicate diurnal oscillations in northerly winds which undergo a modulation of approximately ±30% in amplitude about a mean value of 50–70 m s^{-1}, which maximum value in winter. The observed phases do not vary significantly throughout the year. The theoretical model predicts a seasonal variation of northerly velocity in the upper thermosphere of about 42±12 m s^{-1} during SSMIN, and about 65±5 m s^{-1} during SSMAX, where the greater amplitudes occur during winter for SSMIN and summer for SSMAX. Since the above observations were collected during the decline of a rather weak solar maximum, comparison with the SSMIN theoretical results, which are consistent with the observed variations, is probably appropriate.

Vertical and horizontal structures of the temperature and vertical velocity fields are depicted in Figs. 5–7 for December solstice conditions. Above 200 km a fairly consistent pattern develops for diurnal oscillations in w and δT. The amplitude of w in summer exceeds that in winter by a factor of 2 more or less, depending on latitude. This pattern exists for diurnal oscillations in temperature to a lesser degree; the increased adiabatic cooling associated with the w field during summer as opposed to winter, which is nearly in phase (~1200 h) with the EUV heat source, acts to suppress the seasonal variations in the diurnal tidal

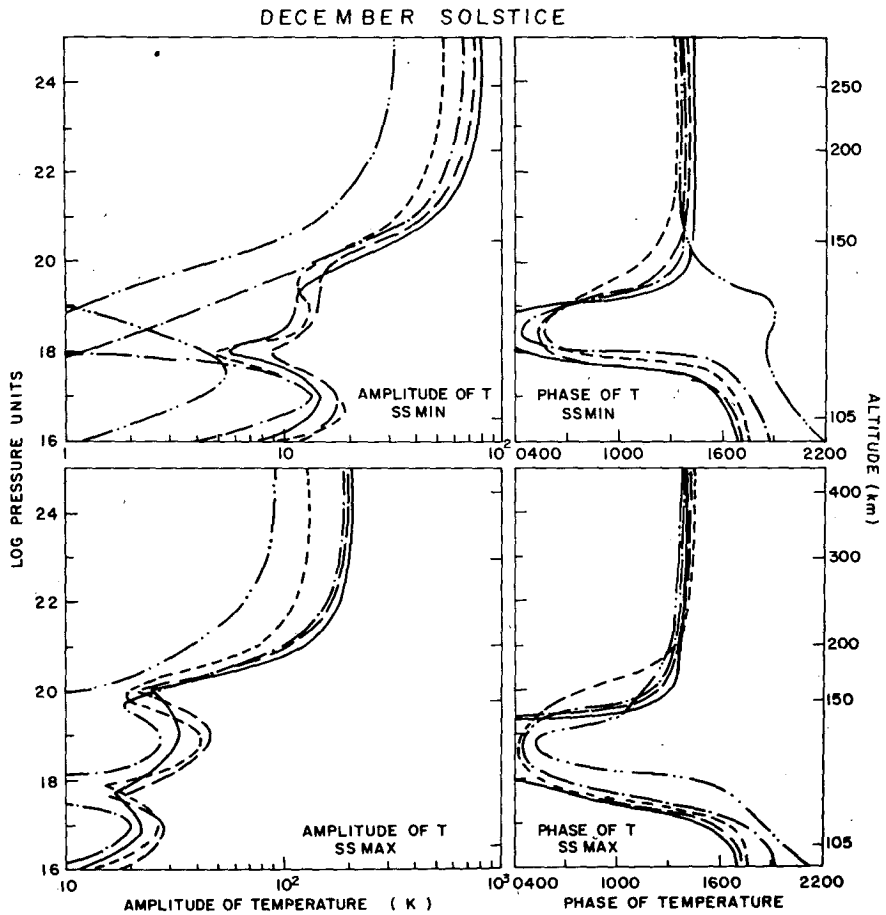

FIG. 5. As in Fig. 3, except for temperature.

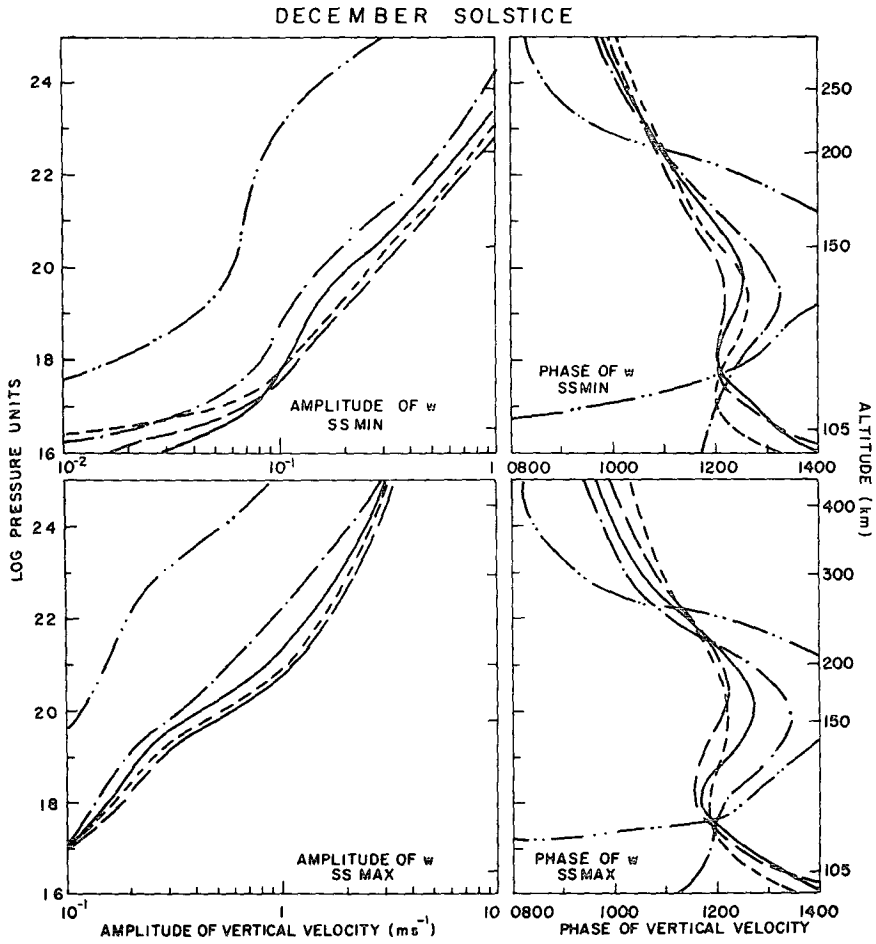

FIG. 6. As in Fig. 3, except for vertical velocity.

oscillation in temperature. In the lower thermosphere the seasonal variability in vertical velocity is somewhat more pronounced, and the phase of the winter oscillation lags behind the summer by 1–6 h depending on latitude. The asymmetric component of δT becomes particularly prominent in the lower thermosphere during SSMAX, with a phase shift of 3–6 h between winter and summer.

Midlatitude incoherent scatter observations (Salah, 1974; Fontanari and Alcayde, 1974) do not contain any detectable seasonal variation of the diurnal amplitude of δT in the upper thermosphere. However, the Millstone Hill data do indicate systematically earlier phases during summer ($\sim$1300 local time) as opposed to winter ($\sim$1400). The theoretical model predicts seasonal variations in the diurnal amplitude of δT at 45°N of approximately $\pm 15\%$ about mean value of 50 K at SSMIN and 150 K at SSMAX, with the greater values occurring in summer. These variations are probably too small, at least during SSMIN, to be reliably detected in the amount of data currently available. Note from Fig. 7 that the phase of δT at 300 km does not vary significantly with latitude according to theory. In the lower thermosphere the phase of δT during winter generally lags behind the summer oscillation by several hours.

b. *Tidal variations in* O *and* N_2

Latitude structures of diurnal oscillations in O and N_2 at 150 and 300 km for SSMIN and SSMAX are depicted in Fig. 8. The O and N_2 distributions at 300 km generally exhibit enhanced densities in the summer hemisphere, consistent with the abundant satellite drag (Jacchia and Slowey, 1968) and mass spectrometer data (Hedin *et al.*, 1974) which have been analyzed. In the lower thermosphere a double-peaked structure appears, with maxima at latitudes ranging from 10° to 60°. Sufficient low-altitude data are not available to confirm this latter prediction. The phase of O almost always lags that of N_2—the phase difference becoming relatively greater at lower altitudes, summer latitudes and high solar activity. The variation of the phase difference with height is due to the effects of wind-induced diffusion (Mayr and Volland, 1972, 1973), which dominates the diurnal variation of O at lower altitudes, and becomes less important at high altitudes where both the O and N_2 variations approach diffusive equilibrium.

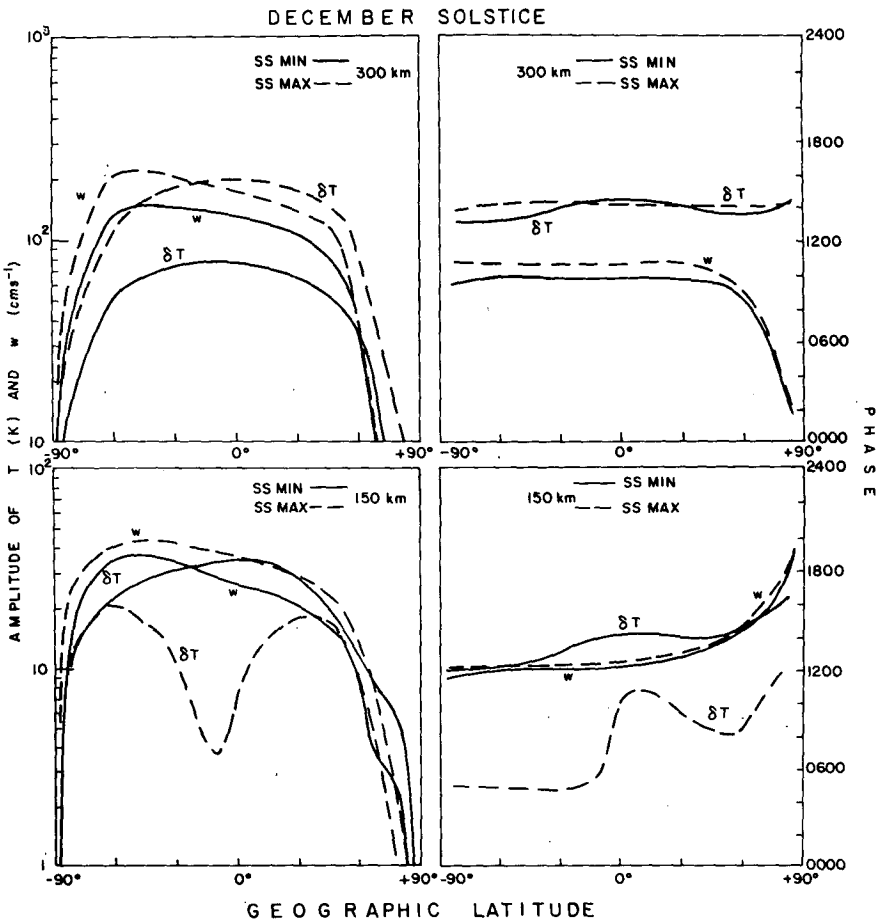

FIG. 7. Horizontal structures of vertical velocity and temperature at 300 km (top) and 150 km (bottom) for SSMIN and SSMAX. December solstice conditions are assumed.

Perhaps the most well-known phenomenon related to tidal variations in upper atmosphere composition is the so-called "phase anomaly" between upper thermosphere density and temperature. As discussed above, previous investigators have demonstrated that this phenomenon is due to the effects of wind-induced diffusion in determining diurnal variations in atomic oxygen, which dominate over N_2 variations above 200 km. The present model provides new information regarding the seasonal and solar cycle variability of this effect. In Fig. 9 the δT-O phase difference is plotted at 300 km for SSMIN and SSMAX. The temperature phase generally leads that of atomic oxygen by several hours, with the exception of high winter latitudes. Furthermore, the phase difference decreases from summer to winter, and increases with level of solar activity. The smaller phase difference at a given height for SSMIN as opposed to SSMAX is related to the increased importance of molecular diffusion during SSMIN, whereas the winds are not appreciably solar-cycle dependent, as discussed in Section 3b. We emphasize that the phase anomaly described here is relative solely to diurnal oscillations, and a complete description of the phenomenon, and comparison with observations, must take into consideration the effects of semidiurnal and possibly terdiurnal contributions.

4. Summary and conclusions

The linearized tidal equations for a spherical rotating, viscous atmosphere with anisotropic ion drag are integrated numerically to determine the seasonal-latitudinal variability of the diurnal thermospheric tide for minimum and maximum levels of solar activity. There are two aspects of the physical model which should be mentioned. First, composition variations at a given height are neglected when computing the tidal variations in u, v, w and T; the variations of O and N_2 are computed *a posteriori* by considering the tidal winds and temperatures as forcing terms in the vertical momentum and continuity equations for these constituents. This procedure is justified since the tidal solutions asymptote to their diffusion-dominated values below the level, where $[O]\sim[N_2]$ [$\sim$200 km (cf. Forbes and Garrett, 1976)], and has furthermore been substantiated by the binary gas

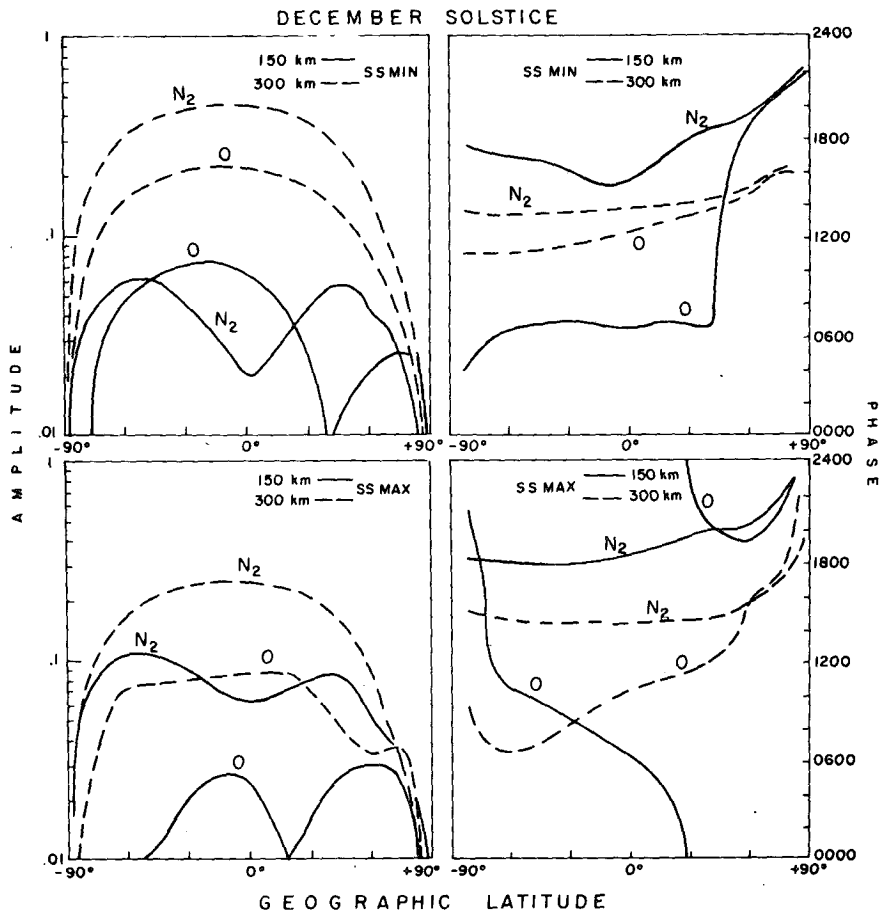

FIG. 8. Horizontal structures of O and N_2 diurnal tidal variations for SSMIN (top) and SSMAX (bottom) at 150 km and 300 km. December solstice conditions are assumed.

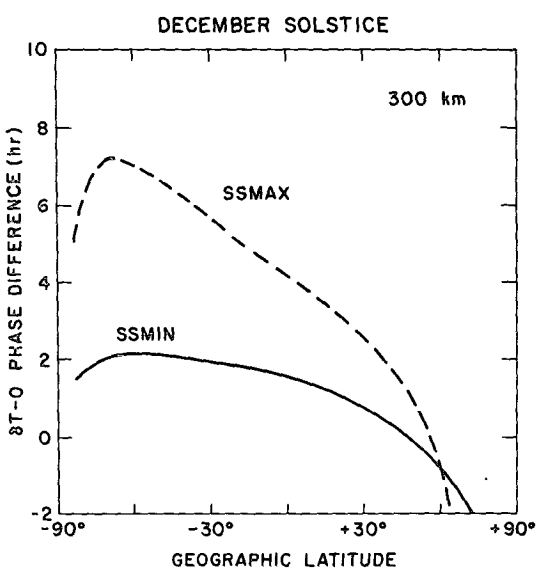

FIG. 9. Phase difference between diurnal tidal oscillations of atomic oxygen and temperature at 300 km for SSMIN and SSMAX. December solstice conditions are assumed.

model of Mayr and Volland (1973). Second, the thermal excitation does not assume the zonally averaged distribution of the absorbing gases to vary with latitude, however, as a consistent tidal calculation would require consideration of mean wind and temperature distributions which are height and latitude dependent. These effects will be included in the numerical model when reliable representations of the zonally averaged wind, temperature and composition distributions become available.

Variations in F-region ionospheric structure and the solar zenith angle dependence of the EUV heat source are major factors controlling the seasonal-latitudinal structure of the diurnal thermospheric tide. The combined interaction of the solar-cycle dependent background temperature profile (which controls the altitude of diffusion dominance), and variations in the seasonal structure of the ionospheric plasma with sunspot activity, leads to a solar-cycle variation of the seasonal-latitudinal morphology of the diurnal tide. For instance, seasonal differences in the tidal winds at a given height are twice as large during

SSMAX as opposed to SSMIN. At a given level of solar activity, westerly winds, vertical winds and temperatures are generally larger in the summer hemisphere, whereas the reverse is true for the northerly wind. There also exist summer-winter phase differences in the tidal fields ranging from 1 to 6 h, depending upon height, latitude and sunspot activity. Computations of diurnal oscillations in O and N_2 are presented which similarly demonstrate a complex dependence of tidal effects on height, latitude, season and solar activity. In particular, the δT-O phase difference (the so-called phase anomaly) at 300 km varies from about 7 to -2 h at SSMAX and 2 to -2 h at SSMIN, between 80°S and 80°N, respectively, at December solstice.

It has been demonstrated that seasonal latitudinal differences in tidal structures and composition variations are most pronounced in the lower thermosphere (100–200 km). Incoherent scatter observations of diurnal tidal phenomena are difficult to obtain in this altitude region due to nighttime sensitivity limitations imposed by low ambient plasma densities. Furthermore, although considerable *in situ* data on lower thermosphere structure is being collected and analyzed from experiments aboard the Atmosphere Explorer series of satellites, the data are not plentiful enough to recover much of the height, latitude, seasonal and solar-cycle structural dependences of diurnal and semidiurnal tides. However, since the present theoretical model is believed to maintain an internal consistency which is realistic, it can be used as an aid in interpreting these data, and "filling in" the structure between statistically reliable data points. Furthermore, the present analysis of seasonal-latitudinal and solar-cycle variations in tidal structure provides needed inputs into numerical investigations of related variations in midlatitude ionospheric structure, the F-region equatorial anomaly, the distributions of O, O_2, N_2, Ar, He and H in the thermosphere, and magnetic and electric field distributions generated by the E-region dynamo mechanism. While such investigations are definitely warranted, they are out of the scope of the present paper.

Due to the inclusion of internally consistent dynamics, solar-cycle, latitude, height and seasonal variations in O and N_2 do not follow that of temperature except in the upper thermosphere. Thus, static diffusion models based on families of empirical temperature profiles cannot simultaneously yield realistic diurnal variations in O, N_2 *and* temperature below 200 km for SSMIN and 300 km for SSMAX.

Acknowledgments. J. M. Forbes gratefully acknowledges financial support under Grant AFOSR 77-3223 from the Air Force Office of Scientific Research to Boston College. The efforts of Meg Hurley in preparing the figures and Mary Kelly in typing the manuscript are greatly appreciated.

REFERENCES

Amayenc, P., 1974: Tidal oscillations of the meridional neutral wind at midlatitudes. *Radio Sci.*, **9**, 281–294.

Ching, 1975: An improved phenomenological model of ionospheric density. *J. Atmos. Terr. Phys.*, **37**, 1563–1570.

Ching, B. K., and Y. T. Chiu, 1973: A phenomenological model of global ionospheric electron density in the E-, F_1- and F_2-regions. *J. Atmos. Terr. Phys.*, **35**, 1615–1630.

Dickinson, R. E., E. C. Ridley and R. G. Roble, 1975: Meridional circulation in the thermosphere. I. Equinox conditions. *J. Atmos. Sci.*, **32**, 1737–1754.

Fontanari, J., and D. Alcayde, 1974: Observation of neutral temperature tidal-type oscillations in the F_1 region. *Radio Sci.*, **9**, 275–280.

Forbes, J. M., and H. B. Garrett, 1976: Solar diurnal tide in the thermosphere. *J. Atmos. Sci.*, **33**, 2226–2241.

——, and R. S. Lindzen, 1976: Atmospheric solar tides and their electrodynamic effects—I. The global Sq current system. *J. Atmos. Terr. Phys.*, **38**, 897–910.

Garrett, H. B., and J. M. Forbes, 1978: Tidal structure of the thermosphere. Submitted to *J. Atmos. Terr. Phys.* (in press).

Geisler, J. E., 1967: A numerical study of the wind system in the middle thermosphere. *J. Atmos. Terr. Phys.*, **29**, 1469–1482.

Harris, I., and H. G. Mayr, 1975: Diurnal variations in the thermosphere 1. Theoretical formulation. *J. Geophys. Res.*, **80**, 3925–3933.

Hedin, A. C., H. G. Mayr, C. A. Reber, N. Spencer and G. R. Carignan, 1974: Empirical model of global thermospheric temperature and composition based on data from the OGO quadrupole mass spectrometer. *J. Geophys. Res.*, **79**, 215–225.

Hilsenrath, J., C. W. Beckett, W. S. Benedict, L. Fano, H. J. Hoge, J. F. Masi, R. L. Nutall, Y. S. Touloukian and H. W. Woolly, 1960: *Tables of Thermodynamic and Transport Properties.* Pergamon Press, 478 pp.

Hong, S. S., and R. S. Lindzen, 1976: Solar semidiurnal tide in the thermosphere. *J. Atmos. Sci.*, **33**, 135–153.

Jacchia, L. G., and J. W. Slowey, 1968: Diurnal and seasonal latitudinal variations in the upper atmosphere. *Planet. Space Sci.*, **16**, 509–524.

Kohl, H., and J. W. King, 1967: Atmospheric winds between 100 and 700 km and their effects on the ionosphere. *J. Atmos. Terr. Phys.*, **29**, 1045–1062.

Lindzen, R. S., 1976: A modal decomposition of the semidiurnal tide in the lower thermosphere. *J. Geophys. Res.*, **81**, 2923–2926.

——, and H. L. Kuo, 1969: A reliable method for the numerical integration of a large class of ordinary and partial differential equations. *Mon. Wea. Rev.*, **97**, 732–734.

Marcos, F. A., H. B. Garrett, K. S. W. Champion and J. M. Forbes, 1977: Density variations in the lower thermosphere from analysis of the AE-C accelerometer measurements. *Planet. Space Sci.* (in press).

Mayr, H. G., and H. Volland, 1972: Diffusion model for the phase delay between thermospheric density and temperature. *J. Geophys. Res.*, **77**, 2359–2367.

——, and ——, 1973: A two-component model of the diurnal variations in thermospheric composition. *J. Atmos. Terr. Phys.*, **35**, 669–680.

——, and I. Harris, 1977: Diurnal variations in the thermosphere. 2. Temperature, composition, winds. *J. Geophys. Res.* (in press).

Richmond, A. D., S. Matsushita and J. D. Tarpley, 1976: On the production mechanism of electric currents and fields in the ionosphere. *J. Geophys. Res.*, **81**, 547–555.

Rishbeth, H., and O. K. Garriott, 1969: *Introduction to ionospheric Physics*, Academic Press.

Roble, R. G., 1975: The calculated and observed diurnal variation of the ionosphere over Millstone Hill on March 23–24, 1970. *Planet. Space Sci.*, **23**, 1017–1030.

——, and R. E. Dickinson, 1973: Is there enough solar extreme ultraviolet radiation to main the global mean thermospheric temperature? *J. Geophys. Res.*, **78**, 249–257.

——, and ——, 1974: The effect of displaced geomagnetic and geographic poles on the thermospheric neutral winds. *Planet. Space Sci.*, **22**, 623–631.

——, J. E. Salah and B. A. Emery, 1977: The seasonal variation of the diurnal thermospheric winds over Millstone Hill during solar cycle maximum. *J. Atmos. Terr. Phys.*, **39**, 503–511.

——, B. A. Emery, J. E. Salah and P. B. Hays, 1974: Diurnal variation of the neutral thermospheric winds determined from incoherent scatter radar data. *J. Geophys. Res.*, **79**, 2868–2876.

Salah, J. E., 1974: Daily oscillations of the midlatitude thermosphere studied by incoherent scatter at Millstone Hill. *J. Atmos. Terr. Phys.*, **36**, 1891–1909.

Straus, J. M., S. P. Creekmore, R. M. Harris and B. K. Ching, 1975a: Effects of heating at high latitudes on global thermospheric dynamics. *J. Atmos. Terr. Phys.* **37**, 1545–1554.

——, ——, ——, —— and Y. T. Chiu, 1975b: A global model of thermospheric dynamics—II. Wind, density, and temperature fields generated by EUV heating. *J. Atmos. Terr. Phys.*, **37**, 1245–1253.

Volland, H., and H. G. Mayr, 1973: A numerical study of three-dimensional diurnal variations within the thermosphere. *Ann. Geophys.*, **29**, 61–75.